EVS24
Stavanger, Norway, May 13 - 16, 2009

Design and Optimization of a Switched Reluctance Motor for an Electric Drive Train

Maarten Vanhove, Thomas Gheysen, Tiene Nobels
GROUP T Leuven Engineering College, Vesaliusstraat 13, 3000 Leuven Belgium, tiene.nobels@groept.be

Abstract

In an electric or hybrid vehicle the drive train is the most decisive engineering factor. The choice and design of the electric motor has to be thoroughly examined and well-founded on firm grounds. In this paper the use of a switched reluctance motor as the main drive unit of an electric vehicle is proposed. For this purpose two methods for sizing the 17.5kW switched reluctance motor have been studied and compared. In order to optimize the motor for the Vision 200, analytical calculations were executed resulting in a higher torque density (9086Nm/m^3 compared to 7827Nm/m^3). Extensive finite element analysis has been carried out to adapt the geometry of both designs. Also an attempt was made to reduce the torque ripple which is one of the most important setbacks of the machine. A reduction of the torque ripple of 7.5% was achieved. Using the PC-SRD software the efficiency and dynamic properties of both topologies have been verified, resulting in the choice for the Krishnan methodology.

Keywords: electric motor, design, switched reluctance motor

1 Introduction

In response to the increasing global environmental commitment, volunteers from all over the world assembled in the Vehicle Design Summit (VDS), an international cooperation with the purpose to develop the VDS Vision 200 (Figure 1) and "to catalyze an Energy Space Race : to identify the key characteristics of events like the race to the moon or civil rights movement and then transpose this energy, passion, focus and urgency to the multitude of global challenges (and opportunities) facing humanity and the planet in this day and age". This project concerns the design and production of an efficient five passenger plug-in hybrid vehicle earmarked for India with 95% reduction in life cycle cost [1]. The Vision 200 will be driven by an electric motor, the energy for which is being supplied by batteries and interchangeable auxiliary power units, e.g. hydrogen or bio-ethanol.
Although students lack experience, they have the possibility to innovate unbiased without being held accounted for by shareholders or limited by proprietary agreements. This is shown in many student teams competing in formula car races or solar car races [2]. The VDS goal, however, isn't a single race but a production-ready car for mass production. About 30 university teams all over the world cooperate in order to achieve this goal. GROUP T hosts two teams, of which the motor team presents their results in this paper.

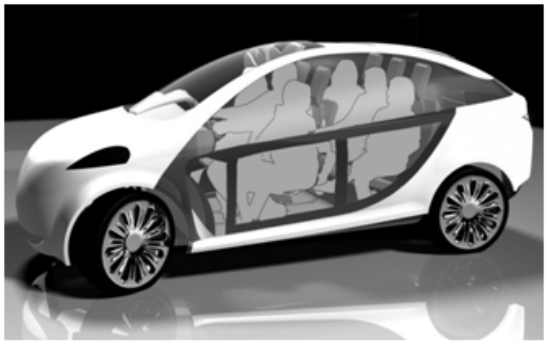

Figure 1: Concept design of the Vision 200

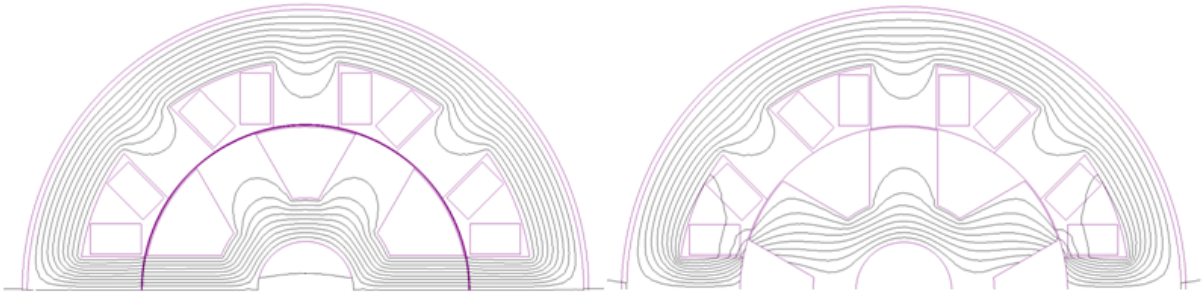

Figure 2: Magnetic flux pattern in aligned (left) and unaligned (right) rotor position

2 Motor selection

The required power for the motor has been determined from typical traffic load diagrams. The estimated vehicle weight amounts to 650kg unloaded (1000kg loaded), top speed equals 80km/h or more, slopes up to 20% and an acceleration from 0 to 100km/h in 13s resulted in a required power of 17.5kW nominal (30kW peak) as also has been presented in [3]. The possibility of using two or four in-wheel motors has been considered but not withheld. A central motor will drive the wheels via a transmission, allowing to increase the nominal speed of the motor (2000 rpm, max 6000 rpm) for lower weight. Table 1 presents the initial electric requirements of the motor.

Table 1: Main electric parameters of the motor

Parameter	Value
P_{nom}	17.5kW
P_{max}	30kW
U_{nom}	360V
U_{max}	380V
I_{nom}	28A
I_{max}	45.3A
T_{nom}	40Nm
T_{max}	70Nm
n_{nom}	2000rpm
n_{max}	6000rpm

A motor type comparison, based on both technological and economical criteria [4], [5], [6], [7], resulted in a choice for the switched reluctance motor (SRM) over the permanent magnet synchronous machine, induction motor or brushless DC motor.
In this doubly-salient, singly-excited motor no windings are needed on the rotor, resulting in lower thermal loading and a lower production cost [8]. The switched reluctance motor has salient poles on both the rotor and the stator and operates like a variable-reluctance stepper motor except for the fact that the phase current is switched on and off as the rotor is at precise positions, which may vary with speed and torque. The operation principle is based on the difference in magnetic reluctance between aligned and unaligned rotor position (Figure 2). By exciting a stator phase the rotor experiences the reluctance force, causing movement to the aligned position. A robust construction and fault tolerant operation are the two most important advantages of a switched reluctance drive.
This motor has, however, several disadvantages resulting in a low penetration in industry [9]. Torque ripple is one of the most important problems of this motor. Especially in the lower speed range, this ripple is experienced as annoying to the driver. Resonance problems and acoustic noise generation origin in torque ripple. Several design and control approaches have been presented in the existing literature to resolve this [10], [11], [12]. However these optimizations do come at a cost, the loss of efficiency being the major setback.
Despite the drawbacks mentioned above, the SRM has been chosen for electric vehicle (EV) propulsion. The first design of this motor for EV applications was presented in [13], where an SRM was designed for high efficiency operation and a prototype was built. Test results showed that the SRM was superior in operation compared to the induction motor; it also had a higher power density than the induction motor.
This paper especially addresses the electromagnetic design issues and presents steady state simulated performance data. Also several alternate designs reducing torque ripple are examined.

3 Machine design

The design of an SRM starts with the selection of the number of stator poles N_s and number of rotor poles N_r. Table 2 presents the possible combinations of N_r and N_s and their properties [14]. Here is m the number of phases, μ the number of active pole pairs per phase and ϵ the duty cycle of the machine topology. The first three combinations cannot start independent, thus they are not interesting. If N_r is higher than N_s, it is proven that torque ripple will be lower, however at a cost of a lower average torque. With ω_{rm} the maximum speed of the motor, the maximum stator

Table 2: Possible combination of N_r and N_s

m	N_s	N_r	μ	$\epsilon(^\circ)$	Strokes/revolution
1	2	2	1	180	2
2	4	2	1	90	4
3	6	2	1	69	6
3	6	4	1	30	12
3	6	8	1	15	24
3	12	8	2	15	24
3	18	12	3	10	36
3	24	16	4	7.5	48
4	8	6	1	15	24
4	16	12	2	7.5	48
5	10	4	1	20	18
5	10	6	1	12	30
5	10	8	1	9	40
5	10	8	2	18	20
6	12	10	1	6	10
6	24	20	2	3	120
6	12	14	1	4.29	84
7	14	10	1	5.14	70
7	14	12	1	4.29	84

frequency can be written as

$$f_s = \frac{\omega_{rm}}{2\pi} N_r. \tag{1}$$

A higher amount of rotor poles implies that f_s will increase, resulting in increased iron losses. The $N_r = N_s - 2$ combinations has been proven to have the best results in practice. Choosing an optimum between low construction and controlling complexity on the one hand and low torque ripple on the other hand, resulted in 8 stator poles and 6 rotor poles.
The choice of the lamination material was based on practical experience. The silicon steel M19 (26 Gauge) has been selected because it is the most common grade for motion control products, as it offers nearly the lowest core loss in this class of materials, with only a small cost impact, particularly in low to medium production quantities. In the existing literature several methods for designing SRMs have been presented. Two of these methods have been researched and compared [15], [16].

3.1 Krishnans method

The method described in [17] starts with the derivation of the motor power P_d

$$P_d = \eta \epsilon k_1 k_2 B A_{sp} D^2 L N_r \tag{2}$$

as the primary machine formula, where η is the machine efficiency, ϵ is the duty cycle defined in (4), k_1 and k_2 are constants given by (5) and (6), B is the flux density at aligned position, D is the bore diameter, L is the stack length of the laminations and A_{sp} is the specific electric loading which is defined as

$$A_{sp} = \frac{2 T_{ph} i m}{\pi D}, \tag{3}$$

where T_{ph} is the number of turns per phase and m is the number of phases that conduct simultaneously and i is the peak stator current.
Defining

$$\epsilon = \frac{\theta_i q P_r}{360}, \tag{4}$$

$$k_1 = \frac{\pi^2}{120}, \tag{5}$$

$$k_2 = 1 - \frac{1}{\sigma \lambda_u}. \tag{6}$$

σ and λ_u are given by

$$\sigma = \frac{L_a^s}{L_a^u}, \tag{7}$$

$$\lambda_u = \frac{L_a^u}{L_u}, \tag{8}$$

where L_a^s,L_a^u and L_u are defined in figure 3 as the inductances at aligned (saturated and unsaturated) and unaligned position respectively.

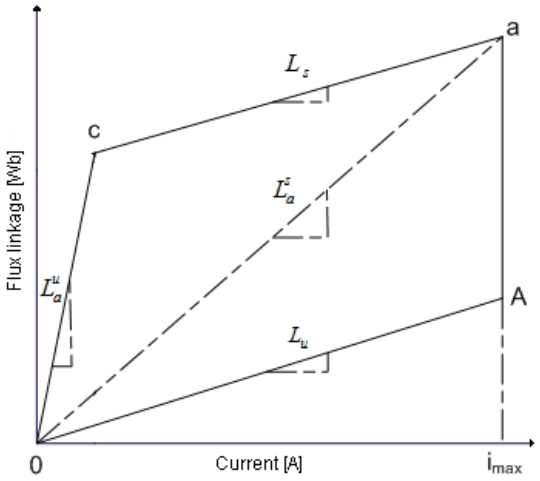

Figure 3: Flux linkage vs. stator current

From the machine formula (2) an equation for the machine torque can be deviated, given by

$$T = \frac{\pi}{4} k_d k_e k_2 B A_{sp} D^2 L. \tag{9}$$

Using formula (2) the power developed by the motor can be written in function of the bore diameter using $L = kD$. The ratio of the lengths to bore k need not be arbitrary; it is decided by the nature of the application and space constraints. Figure 4 gives the relationship between D, L and k using the machine formula. The other parameters in 2 have, using practical experience, a minimum and maximum value. This results in two

lines which are plotted. The surface enclosed by these two lines, gives the possible combinations for L and D. Due to space constraints $k = 1.5$ is chosen.

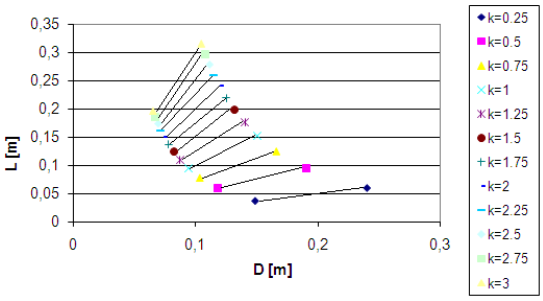

Figure 4: Possible combinations of L and D

The other dimensions, presented in figure 5, are determined to accommodate the maximum of the magnetic field density in the corresponding segment of the motor.

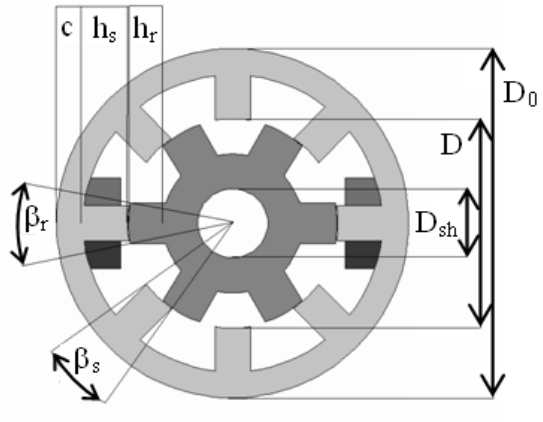

Figure 5: Motor model

3.2 Vijayraghavans method

A second method for the initial calculation of the motor dimensions is presented in [16]. This method starts from an equivalent induction motor. From the standard sizes of the frame (F) defined in [18] a first estimation of the stator outer diameter is

$$D_0 = 2(F - 3). \tag{10}$$

From this initial bore diameter, the other dimensions are calculated to accommodate the maximum flux density. The outcome of both design methods is presented in table 3.

3.3 Analytical analysis

The average motor torque has been calculated analytically. Krishnan defines 7 flux paths which need to be examined using the equivalent magnetic circuit of each path [15]. The magnetomotive force (F_1) for each segment of the flux path is evaluated using the B-H characteristics of the lamination material and average length of the flux path in the segments. The stator pole flux density B_{sp} is calculated iteratively with Ampères law,

$$F_1 = T_{ph} i = \sum Hl. \tag{11}$$

With the resulting value of B_{sp}, the inductance (L) of each flux path is calculated and by summing the total inductance of the considered rotor position is found. The flux linkage for this rotor position can be written as

$$\psi = Li, \tag{12}$$

where i is the stator current. Repeating this process for different values of the current and for both aligned and unaligned position results in figure 3.
The work done at aligned position is equal to the surface O, i_{max}, a, C, O (figure 3), or

$$W_a = \int_0^i \psi(\theta, i) di \tag{13}$$

The work done at unaligned position is equal to the surface O, i_{max}, A, O, or

$$W_u = \frac{1}{2} i_p \psi_u = \frac{1}{2} i_{max}^2 L_u, \tag{14}$$

with i_{max} the peak value of the current. The total amount of work W done by the motor is the difference between W_a and W_u, consequently that the average torque of the motor can be written as

$$T_{av} = \frac{W N_s N_r}{4\pi}. \tag{15}$$

Table 3: Basic motor dimensions, Krishnans and Vijayraghavans method

	Vijayraghavan	Krishnan
Bore diameter, D	160mm	130mm
Stator pole height, h_s	51.87mm	24.9mm
Rotor pole height, h_r	42.71mm	29.7mm
Airgap, g	0.5mm	0.5mm
Shaft diameter, D_{sh}	42mm	38mm
Stator yoke, C	25.13mm	20.5mm
Stator outer diameter, D_0	314mm	220mm
Stator pole angle, β_s	18°	18°
Rotor pole angle, β_r	20°	20°
Turns per phase, T_{ph}	90	82
Stack Length , L	200mm	200mm

4 Optimization

Both designs have been verified and optimized using finite element analysis (FEA). This section presents the results of these optimizations.

4.1 Stator- and rotor pole torque optimization

First the influence of the stator and rotor pole angles (β_s and β_r, figure 5) on the average torque is examined. These angles, however, should comply with three conditions necessary for guaranteeing high aligned inductance, independent starting and avoiding overlap in unaligned position, which results in a range of allowed combinations for β_s and β_r [15].
Figure 6 presents the analytical results of Krishnans model, the outcome of Vijayraghavans model has the same results, namely the best combination is $\beta_s = 23°$ and $\beta_r = 24°$. However, the torque to volume ratio of Vijayraghavans model lies significantly lower.

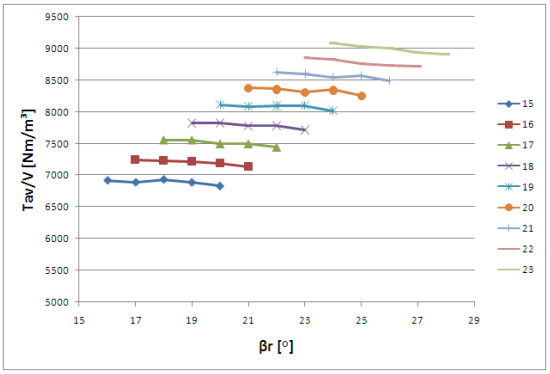

Figure 6: Average torque to volume ratio for different pole angle combinations

4.2 FEA optimization

To verify the analytical results, FEA was used to determine the steady state performance data of both topologies. FEA gives a very accurate assessment of electromagnetic properties of the motor. Figure 7 presents the 2D-mesh of the SRM delivered by MAGNET.

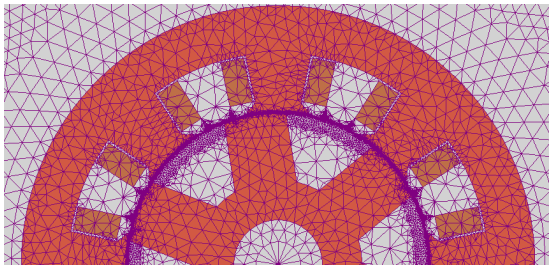

Figure 7: Mesh of the Krishnan topology delivered by MAGNET

MAGNET FEM software delivered the stator coil flux linkages as a function of current and position (Figure 8). By comparing the FEA results with the analytical calculations it was verified that the analytical approach was a good estimation. The electromagnetic reluctance torque equals the derivative of the magnetic coenergy

$$T(i,\theta) = \frac{\partial W_{co}(i,\theta)}{\partial \theta} = \int_0^i \frac{\psi(i,\theta)}{\theta} di, \quad (16)$$

which on its turn is the surface between the flux linkage-current curves in aligned and unaligned position.

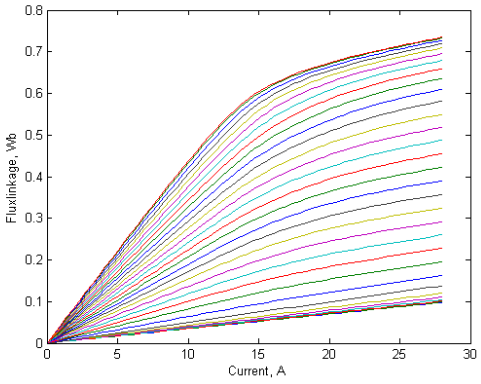

Figure 8: Flux linkage of the SRM

Figure 9 combines the torque-position curves of all the four phases and the resulting rippled machine torque. Because mutual inductance between phases is very low, superposition could be applied to find the machine torque. In comparison with complete dynamic analysis, this method has been proven to be a fruitful approach for calculating the other torque-position curves [19]. The results of both models are plotted.

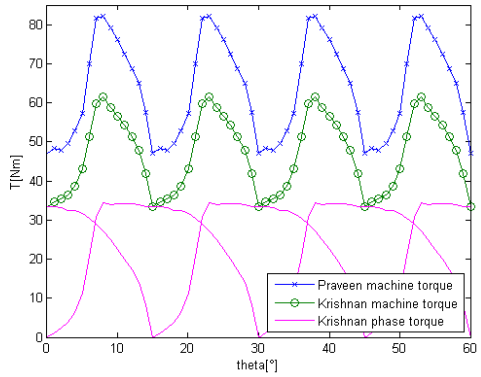

Figure 9: Reluctance torque combined for the four different phases

In order to achieve a reduction in torque ripple, geometric adjustments have been researched. First the effect of an altered stator pole is examined. The tip of the stator tooth is changed such that the magnetic flux will have a preferred direction, minimizing the abrupt transition between phases which results in a lower torque ripple. Second the stator pole was rounded off to minimize the magnetic resistance in the motor. Figure 10 presents the altered stator teeth, with α_r

as the rounding radius of the stator teeth, γ_{r1} and γ_{r2} the radii of the stator pole tip alteration.

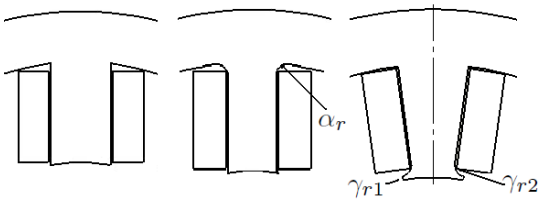

Figure 10: Standard stator tooth (left), rounded stator tooth (middle) and tip adjustment (right)

The same FEA method has been used to verify these design modifications. The results have been plotted in figure 11. It can be noted that there is almost no difference between the standard configuration and the rounded stator teeth.

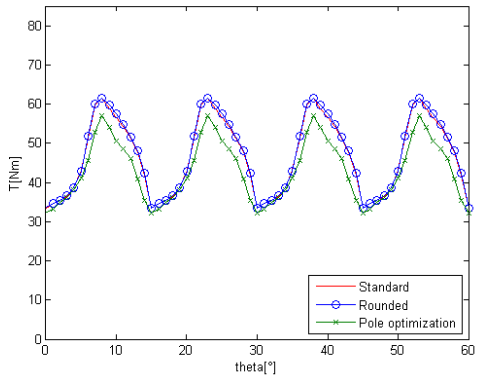

Figure 11: FEA results of design modifications

The altered stator tip seems the most fruitful approach, the torque ripple has been reduced from 30.4Nm to 25.2Nm . However, this optimization comes at a cost. The average torque has also been reduced from 47.8Nm to 43.7Nm.

4.3 PC-SRD optimization

The analytical program PC-SRD, developed by the SPEED consortium, was used to determine the dynamic performance of the motor, namely the torque-speed curves and the peak efficiency [20]. As this software is unable to verify the results of the altered stator tip geometry, the basic model of both topologies has been examined.
Figure 12 presents the torque-speed curve of Vijayraghavans model and figure 13 plots the torque-speed curves of the Krishnan prototype (blue).
PC-SRD also provided a peak efficiency of 92.15% at base speed (2000rpm), this does not include the efficiency of the control unit.

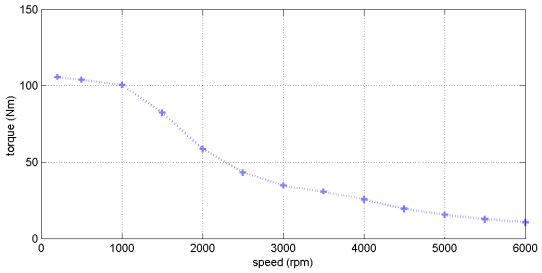

Figure 12: Torque-speed curve of Vijayraghavans model

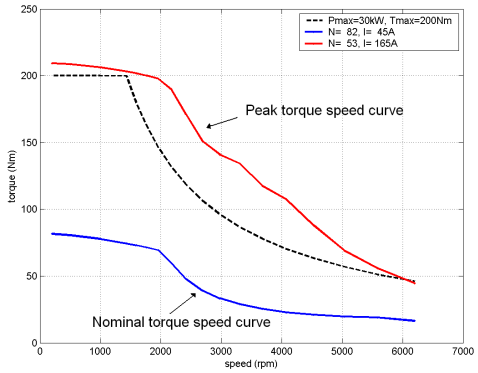

Figure 13: Torque-speed curve of Krishnans model

5 Discussion

A significant difference is noted between the two design methods described above. Vijayraghavans model is exceedingly bigger, which results in a higher torque development. However, the torque to volume ratio of Krishnans topology lies clearly higher . This is partly due to the fact that Vijayraghavan starts the design from an equivalent induction motor, which has been proven to have a lower power density than an SRM [13].
The influence of different combinations of pole angles on the average torque was examined. From figure 6 the optimal combination of $\beta_s = 23°$ and $\beta_r = 24°$ can be concluded. These angles result in the highest torque to volume ratio for both topologies. Again a difference is noted between the two designs, the torque density of Krishnans model almost lies a factor 2 higher (9086Nm/m^3 compared to 5045Nm/m^3).
To lower the torque ripple some changes in the basic motor geometry have been researched. The altered stator tip proves to be the most fruitful approach. It must be said that only a reduction of 7.5%, compared to maximum machine torque, has been realized. Rounding off the stator teeth has almost no effect on the generated torque ripple in the machine. However, because of the manufacturing advantage the final motor design still contains these rounded teeth.
Figure 13 plots next to the nominal torque-speed

curve also the peak torque-speed curve and the required peak power specifications (30kW) of the Krishnan design. It can be noted that the nominal torque-speed curve lies significantly lower than the required specs. By increasing the maximum current (to maximum 165A), the required peak power specifications can be met. The maximum power is only needed for acceleration on a ramp with a slope of 20%. For a short time this kind of amperage can be delivered by the power unit (e.g. batteries), however, some further research is needed to design an appropriate cooling jacket.

6 Final design

A motor type comparison concluded that the switched reluctance motor has ideal characteristics to drive the electric drive train of an EV. A simple and robust design and a high torque density confirm these assumptions. This paper examined two different methods for designing an SRM for an EV. The proposed Krishnan model shows superior properties, e.g. a significantly lower mass (57kg compared to 95kg) and a higher torque density. Using FEA the stator poles have been optimized, resulting in a lower torque ripple. Table 4 presents the final dimensions and parameters of the Krishnan motor.

Table 4: Final dimensions and parameters of the optimized Krishnan motor

Parameter	Value
Bore diameter, D	130mm
Stator pole height, h_s	24.9mm
Rotor pole height, h_r	29.7mm
Airgap, g	0.5mm
Shaft diameter, D_{sh}	38mm
Stator yoke, C	20.5mm
Stator outer diameter, D_0	220mm
Stator pole angle, β_s	23°
Rotor pole angle, β_r	24°
Turns per phase, T_{ph}	82
Stack Length , L	200mm
Rounding radius, α_r	5mm
Stator pole tip radius 1, γ_{r1}	1mm
Stator pole tip radius 2, γ_{r2}	4mm
Mass, m	57.2kg
Lamination material	M19, 26 Gauge
Peak efficiency, $\eta_m ax$	92.15%
Average torque, T_{av}	47.81Nm
Peak torque, T_{max}	81Nm
Nominal power, P_{nom}	16.3kW
Peak power, P_{max}	30.6kW
Nominal stator current, i_{nom}	28A
Peak stator current, i_{max}	165A

Acknowledgments

The authors wish to acknowledge the support of Psicontrol Mechatronics and the ELECTA-ESAT research division at K.U.Leuven, in particular the expertise of ir. Kevin Verhaege and dr. ir. Stijn Stevens.

References

[1] VDS. http://www.vehicledesignsummit.org, accessed on 5 - 2007.

[2] WSC. http://www.wsc.org.au, accessed on 7 - 2007.

[3] S. Ramamurthy et.al. Sizing a switched reluctance motor for electric vehicles. *IEEE Transactions on Industry Applications*, 37:1256–1264, 2001.

[4] H.C. Lovatt et. al. Comparative performance of singly salient reluctance, switched reluctance, and induction motors. *Eighth International Conference on Electrical Machines and Drives*, 8:361–365, 1997.

[5] K.M. Rahman et. al. Advantages of switched reluctance motor applications to ev and hev:design and control issues. *IEEE Transactions on Industry Applications*, 36:111–121, 2000.

[6] J. Puranen. *Induction motor versus permanent magnet synchronous motor in motion control applications: a comparative study*. PhD thesis, Lappeenranta University of Technology, 2006.

[7] I. Boldea; S.A. Nasar. *Electric drives*. CRC Press, Florida, 1998.

[8] T.J.E. Miller. *Switched reluctance motors and their control*. Magna Physics Publishing, New York, 1993.

[9] K.M. Rahman. Design of high efficiency and high density switched reluctance motor for vehicle propulsion. *IEEE Transactions on Industry Applications*, 38:1500–1507, 2002.

[10] R.S. Colby et.al. Vibrating modes and acoustic noise in a 4 phase switched reluctance motor. *Conference Record of the 1995 IEEE*, 1:441–447, 1995.

[11] D.E. Cameron et.al. The origin and reduction of acoustic noise in a doubly salient variable-reluctance machine. *IEEE Transactions on Industry Applications*, 28:1250–1255, 1992.

[12] C. Pollock et.al. Acoustic noise cancellation technique for switched reluctance drives. *IEEE Transactions on Industry Applications*, 33:477–484, 1997.

[13] P.J. Blake et.al. The control of switched reluctance motors for battery electric road vehicles. *International Conference on PEVD*, May:361–364, 1984.

[14] G.P.M. Hof. Moderne elektrische aandrijvingen in de transporttechniek. Technical report, TU Delft Faculteit Ontwerp, Constructie en Productie, 2001.

[15] R. Krishnan. *Switched Reluctance Motor Drives: Modeling Simulation, Analysis, Design and Applications*. Industrial Electronics, Florida, 2004.

[16] P. Vijayraghavan. *Design of Switched Reluctance Motors and Development of a Universal Controller for Switched Reluctance and Permanent Magnet Brushless DC Motor Drives*. PhD thesis, Virginia Polytechnic Institute and State University, 2001.

[17] R. Krishnan et.al. Design procedure for switched-reluctance motors. *IEEE Transactions on Industry Applications*, 24:456–461, 1988.

[18] International Electrotechnical Commission. Dimensions and output ratings for rotating electrical machines - frame numbers 56 to 400 and flange numbers f55 to f1080. *IEC*, 72, 1971.

[19] F. D'Hulster. *Optimalisatieplatform voor de koppelregeling van 8/6 SR-motoren*. PhD thesis, K.U.Leuven, 2005.

[20] T.J.E. Miller. *PC-SRD reference manual*. University of Glasgow SPEED Laboratory, 1995.

Authors

Maarten Vanhove is working towards the M.Sc degree in electromechanical engineering from GROEP T - Leuven Engineering College, Leuven, Belgium. In 2007 he joined the VDS-GROUP T team where he is responsible for the design of the electric motor. His research interests include electrical machines design.

Thomas Gheysen is pursuing the M.Sc degree in electromechanical engineering from GROEP T - Leuven Engineering College, Leuven, Belgium in 2009. In 2007 he joined the VDS-GROUP T team where he is responsible for the design of the electric motor. His research interests include electrical machines design and battery management systems.

Tiene Nobels received the M.Sc degree in electrical engineering and the PhD degree from the Katholieke Universiteit Leuven (K.U.Leuven), Leuven, Belgium in 1999 and 2005 respectively. In 2001 she joined GROEP T - Leuven Engineering College, where she is currently a full time lecturer. She teaches electrical engineering and design project courses. Her research interests include electromagnetic simulations and electrical machines design.